ELSEVIER

Nuclear Instruments and Methods in Physics Research B 117 (1996) 367-374

NIM B
Beam Interactions with Materials & Atoms

Multi-wavelength Raman probing of phosphorus implanted silicon wafers

Andreas Othonos, Constantinos Christofides *

Department of Natural Sciences, Faculty of Pure and Applied Sciences, University of Cyprus, P.O. Box 537, 1678 Nicosia, Cyprus

Received 6 July 1995; revised form received 8 March 1996

Abstract

Raman spectroscopy is performed on phosphorus implanted silicon wafers with several excitation laser wavelengths ranging from 458 nm to 752.5 nm. The silicon layers were implanted with various implantation energies and doses, ranging below and over the critical dose of amorphization. A factor κ, relating the Raman intensity of the implanted samples with that of the pure crystalline silicon is introduced, and used to correlate the effects of ion implantation at different doses, different implantation energies and various annealing temperatures, on the silicon lattice.

1. Introduction

Ion implantation is a key technological process in modern microelectronics for the fabrication of shallow p–n junctions. It has been introduced as an alternative to diffusion for the semiconductor doping process. The implantation of impurity atoms presents many advantages such as rapidity, mass separation for purity requirements, accuracy and wide range of doses, flexibility of profile depth and the ability to control the amount of dose in a specific region of a semiconductor. In addition, the bombardment of solids by ion implantation has also been widely used for the study of amorphization and physical analysis of structural disorder introduced by irradiation [1].

Ion implantation is normally followed by annealing in order for the semiconductor to recover its crystallinity and the doping impurity to become active. One of the main problems which remains unsolved in the field of ion-implantation is due to the confusion that exists between the activation of the implanted impurities and the evolution of the structural properties of such inhomogeneous materials during the annealing process [2].

Many kinds of characterization techniques of the implanted layers have been developed during the last three decades. Raman scattering is one such technique: parameters such as intensities, frequencies, line shape and linewidth, can be used to characterize the lattice, impurities and free carriers in a semiconductor material. Seeing the amount of information provided by Raman scattering, such studies are expected to be very fruitful for the understanding of defect formation and dissolution (after annealing process). Characterization of ion implanted semiconductors based on Raman spectra has been reported by a number of researches [3–10]. In the past, Engstrom and Bates [7] as well as Forman et al. [8] studied boron and arsenic-implanted and annealed silicon wafers. Raman spectra on arsenic-implanted and rapidly annealed wafers were also studied by Kirillov et al. [9] and by Nakamura and Katoda [10], who have used the same technique to study Si and Sn implanted GaAs wafers. Recently, Othonos et al. [11] performed Raman and electrical characterization to study the effects of thermal annealing on phosphorus implanted silicon wafers.

In this work Raman scattering is performed on a set of P^+ implanted samples with different wavelengths which correspond in probing the samples with different penetration depths. The aim of this paper is to investigate, by Raman spectroscopy and in particular using the intensity of the silicon phonon peak, four main questions: the scattering for crystalline substrate; the amorphous phase; the mixed amorphous crystalline phase at the initial a/c interface and the distribution of defects as a function of depth.

To our knowledge, this is the first systematic study done on a matrix of thermally annealed P^+ implanted silicon wafers, using multiple wavelengths Raman scattering and specifically using the intensity of the silicon phonon peak at different probing depths as non-destructive characterization of these samples.

* Corresponding author. E-mail: costas@earth.ns.ucy.ac.cy; Fax: +357 2339060.

0168-583X/96/$15.00 Copyright © 1996 Elsevier Science B.V. All rights reserved
PII S0168-583X(96)00304-7

2. Experiment

Next, a brief description of the experimental setup will be given. The beam from the laser source passes through a beam splitter which was set close to Brewster's angle in order to extract only a small portion of the power. This extracted beam, which was approximately 2% of the main laser power, was directed into a meter which allowed continuous monitoring of the incoming laser power. The main beam from the laser was directed in a microscope assembly where it was focused with a 40X times objective on the Si samples. The focus spot on the sample surface was monitored with a ccd camera which helped to maintain the same focusing spot size for all the samples throughout the experiment. The Raman signal was collected with the same objective (in a backscattering configuration) and directed with a beam splitter into a triple-pass Spex monochrometer. This monochrometer consisted of two separate sections: a double monochrometer filter and a single 0.75 m monochrometer. The filter rejected most of the laser light which was only 64.5 meV away from the Raman signal. The final monochrometer was equipped with an 1200 l/mm line grating and its output was directed into a high sensitivity ccd array giving a spectrum of approximately 5 nm wide. In these experiments the Stokes–Raman signal for each of the samples was accumulated over a period of 10 min.

The lower wavelength detection limit which was around 400 nm was set by the optical transmission of our spectrometer and microscope, where the upper limit was set by the sensitivity of our ccd array and the Raman scattering efficiency. The sources used in this work were an Ar ion and a Kr ion lasers. With these lasers it was possible to perform Raman scattering with the following six wavelengths; 458, 488, 531, 568, 647 and 752.5 nm.

3. Experimental results

In this section we describe the results obtained from Raman scattering. Two inch diameter silicon wafers lightly doped with boron (20–25 Ω cm) were used in this study. These samples were implanted through a thin oxide layer at room temperature with phosphorus at various doses and energies. The implanted doses range from 1×10^{13} to 1×10^{16} P^+/cm^2 (W1: 1×10^{13}, W2: 1×10^{14}, W3: 5×10^{14}, W4: 1×10^{15}, W5: 5×10^{15}, W6: 1×10^{16} P^+/cm^2) at constant implanted energy of 150 keV at room temperature. The implanted energies range from 20 to 180 keV (W7: 20, W8: 30, W9: 60, W10: 100, W11: 140, W12: 180 keV) for implanted dose of 5×10^{14} P^+/cm^2. During ion implantation the crystal was oriented in such a way as to minimize channeling effects. After implantation the wafers were cut along the crystallographic axes into several square samples of dimensions 1×1 cm^2. These samples were then thermally annealed isochronically at various temperatures (range of 350 to 1100°C) for one hour in an inert nitrogen atmosphere. After annealing, the oxide overlayer was etched away from these samples. SUPREM simulations had been performed for the above samples in the past and the implanted ion distribution had been estimated. It is important to note that these simulations have been compared with spreading resistance measurements [11].

Raman scattering was performed on these samples with different excitation wavelengths which corresponded in probing the samples with different penetration depths [3] (the optical penetration depth, d, is defined as the depth at which the power of the probing beam is reduced by $1/e$ of its incident value, thus $d = 1/a$, where a is the absorption coefficient). In a perfect silicon lattice the only Raman active mode is the longitudinal optical mode at the centre of the Brillouin zone. This optical phonon is centred at 64.5 meV and it has a Lorentzian shape with 0.5 meV width at room temperature. When the silicon is amorphous, the symmetry is reduced from the crystal space group to the point group of the lattice site. Therefore the Raman signal from an amorphous silicon is related to the phonon density of states, and results in a broad-band feature centered arround 58 meV [11].

The Raman data obtained with the different probing wavelengths have similar spectral features. All spectra for the samples that have some crystalline silicon present within the penetration depth of the probing wavelength show a phonon peak at 64.5 meV (as expected for a silicon crystal). The intensity of this phonon peak depended on the ratio of crystal material to non-crystal through the probing depth. No noticeable change has been observed in linewidth (which was estimated to be 0.5 meV) as well as the position of the silicon phonon peak under the resolution of this experimental system (± 0.1 meV). It appears that the only noticeable change (apart from the amorphous features) was the silicon phonon peak intensity.

As mentioned above using the various laser lines it is possible to change the probing penetration depth and to study the implantation layer of the silicon samples. Thus, for the shorter wavelength where the penetration depth is of the order of the thickness of the ion implantation damaged area the silicon phonon peak intensity will be very small or zero. With increasing penetration depth, as the probing wavelength increases, the silicon phonon peak intensity increases. Eventually as the probing depths become much larger than the implanted layer the contribution from the damage area cannot be detected.

4. Discussion and analysis

This section is divided into two main parts. The first part (4.1) will refer to the results obtained from the samples with different implanted doses of phosphorus, and part (4.2) will refer to results from samples implanted at

different implantation energies. In order to simplify the analysis of the data we will define a factor κ, as the ratio of the phonon Raman peak (*PRP* which is a function of the probing wavelength λ, annealed temperature T_a, dose concentration Φ and ion implantation energy E_0) over the phonon Raman peak for the non-implanted crystalline silicon ($PRP_{cSi}(\lambda)$).

$$\kappa(\lambda, T_a, \Phi, E_0) = \frac{PRP(\lambda, T_a, \Phi, E_0)}{PRP_{cSi}(\lambda)}. \quad (1)$$

This factor will be referred to as the *crystalline factor* for the samples under study and it will take values ranging from 0 to 1. Clearly for a pure crystalline silicon (non-implanted sample) κ will have a value of 1 and for a completely amorphous sample κ will be 0.

4.1. Constant implantation energy samples

The Raman scattering results for the constant implantation energy samples at 150 keV for various doses are summarized in Figs. 1 and 2. In Fig. 1a–c the crystalline factor (κ) is plotted as a function of annealed temperature for some of the different excitation wavelengths. Fig. 2a–d shows the crystalline factor as a function of probing wavelength for some of the silicon samples.

The low doped samples 1×10^{13} P^+/cm^2 have a very strong phonon peak which is indicative of Raman scattering in crystalline silicon samples. The crystalline factor, κ, for the non-annealed sample is approximately 0.78 at the probing wavelength of 458 nm (see Fig. 2a). This factor increases slightly as the probing penetration depth increases with increasing wavelength. The crystalline factor reaches a value of 0.9 at excitation of 752.5 nm, as one would expect, since the probing depth increases thus sampling material that was not effected by the ion implantation. It is clear from the data in Fig. 1 that even mild annealing at 350°C brings the samples close to their maximum crystalline value ($\kappa = 1$). This suggests that the damage caused by the implantation at such small dose is indeed minor (at least for the type of damage that Raman scattering is sensitive to) and these silicon samples may be brought back to their crystalline structure by weak annealing.

The samples with phosphorus doping of 1×10^{14} P^+/cm^2 as seen in Fig. 2b exhibit similar behavior as the previous lower dose samples. The non-annealed sample has a crystalline factor of 0.25 at the probing wavelength of 458 nm which corresponds to approximately 0.5 μm penetration depth [12,13]. The value of the crystalline factor increases with increasing penetration depth and reaches a value of 0.6 at 752.5 nm. The increase in the crystalline factor κ with increasing penetration depth is simply due to the increase in probing depth which effectively covers a region of the sample that is less severely damaged (or undamaged) by ion implantation. One interesting feature in Fig. 2b is the ion implanted region seen in the graph as a dip in the crystalline factor. This dip occurs at the shorter probing wavelengths which correspond to

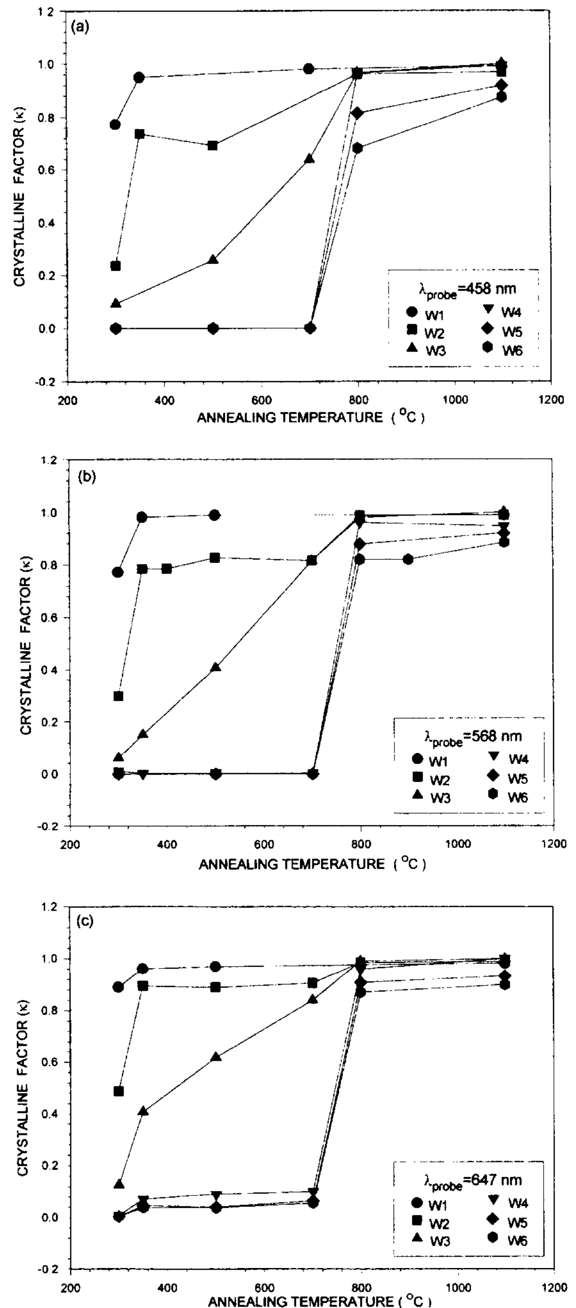

Fig. 1. The crystalline factor κ as a function of annealing temperatures for the constant implantation energy samples W1: 1×10^{13} P^+/cm^2, W2: 1×10^{14} P^+/cm^2, W3: 5×10^{14} P^+/cm^2, W4: 1×10^{15} P^+/cm^2, W5: 5×10^{15} P^+/cm^2, and W6: 1×10^{16} P^+/cm^2. Parts (a) to (c) correspond to 458, 568, and 647 nm probing wavelengths.

shorter probing depth. In other words the dip is located near the surface of the sample and is relatively broad, approximately 1.5–2 μm in length, indicative of ion implantation damage to the crystalline structure of the samples as a function of depth. This feature also appears for the low annealed temperature samples however it is less pronounced. Another interesting point to be made about these samples is their behavior as a function of annealed temperature seen in Fig. 1. It seems that under mild annealing (350°C) the crystalline factor undergoes a large transition. For example in Fig. 1b it starts from 0.3 and after mild annealing it reaches a value of approximately 0.8. This indicates that the perturbation of the samples crystal structure is small and reversible under annealing of only 350°C. In these samples the transition (as seen from the Raman signal, see Fig. 1) of $\kappa < 1$ to $\kappa = 1$ occurs between 700 to 800°C.

The silicon samples doped with 5×10^{14} P^+/cm^2 phosphorus have a less pronounced phonon peak (for non-annealed and mild annealed samples), as it was expected, since the defect formation in the samples increases with increasing doping level. The crystalline factor for the shortest wavelength (smallest probing penetration depth) of the non-annealed sample is approximately 0.09. This value decreases as opposed to the previous cases with increasing probing wavelength reaching a value of 0.04 at 568 nm and then it starts increasing again with a final value of 0.4 at the longest wavelength (deepest probing penetration depth). This suggests that the damage in the crystal structure caused by the ion implantation in this sample is more severe deeper in the sample rather than near the surface. In addition, this region of damage, as seen from Raman scattering data, is broad and has a very low recovery over the probing penetration depth. However, as these samples are annealed, the damage induced deep into the sample recovers at lower temperatures than the damage caused at shallow depths. The result is a depth profile of the crystalline factor which appears narrower than for the unannealed sample.

These particular doped samples also exhibit some interesting features as a function of annealing temperature as seen in Fig. 1. Rather than having the crystalline factor changing values in large steps under annealing this factor changes gradually as a function of annealed temperature

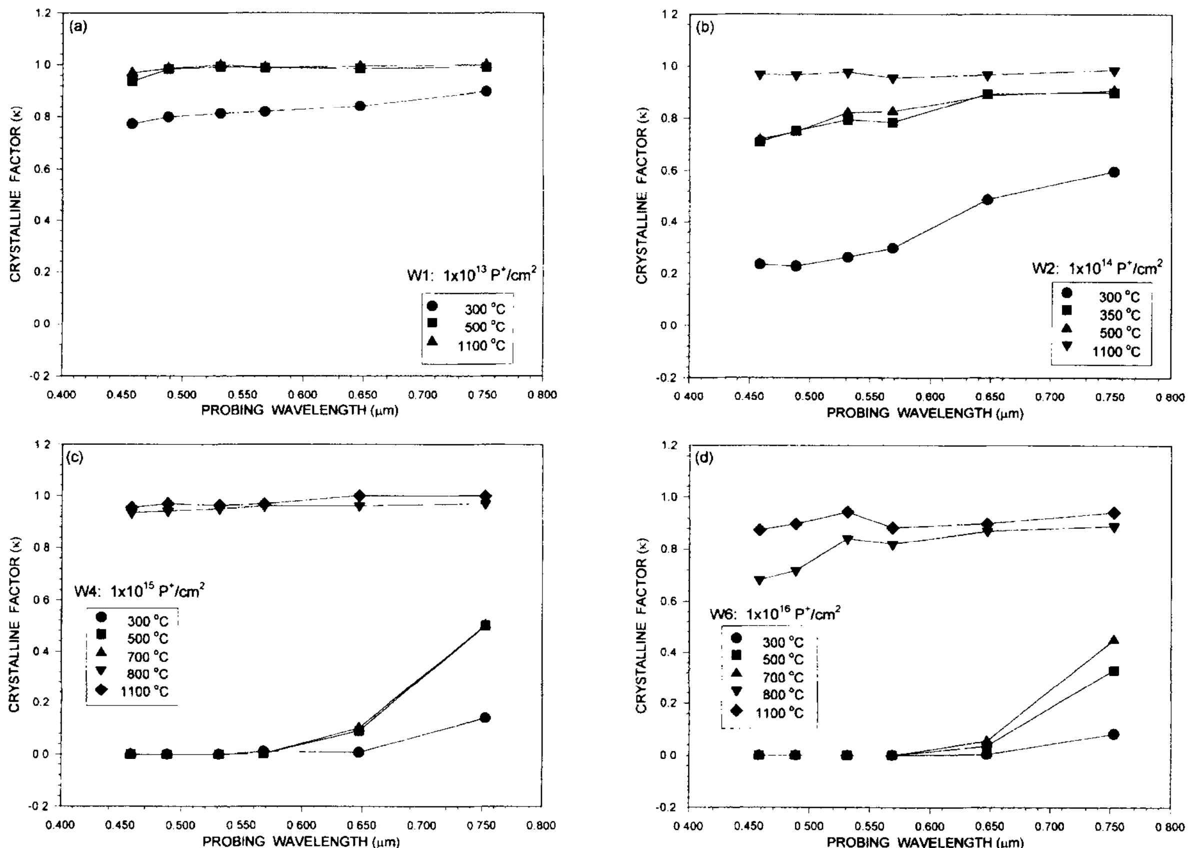

Fig. 2. The crystalline factor κ as a function of probing wavelength for different annealed temperatures. Parts (a) to (d) correspond to some of the different dose implantation samples, namely W1: 1×10^{13} P^+/cm^2, W2: 1×10^{14} P^+/cm^2, W4: 1×10^{15} P^+/cm^2, and W6: 1×10^{16} P^+/cm^2.

reaching a value close to 1 at 800°C. Therefore, the damage induced by the ion implantation for this doped level is reversible. However its temperature dependence is different from the previous samples. In these samples recrystallization occurs gradually with temperature.

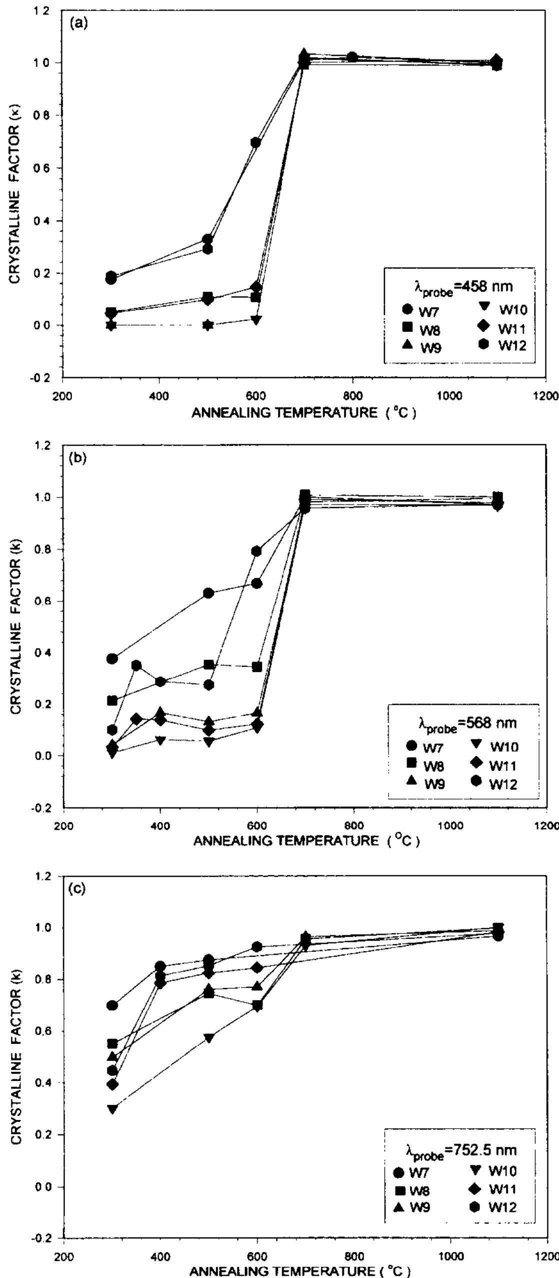

Fig. 3. The crystalline factor κ as a function of the different annealing temperatures for the constant dose samples W7: 20 keV, W8: 30 keV, W9: 60 keV, W10: 100 keV, W11: 140 keV and W12: 180 keV. Parts (a) to (c) correspond to 458, 568 and 752.5 nm probing wavelengths.

Next, let us consider the silicon samples doped with 1×10^{15} P^+/cm^2 phosphorus which is equal to the critical dose of amorphization [14]. For the non-annealed sample, at short penetration depths, the silicon phonon peak is not present. This is expected since the ion implantation above the critical dose results in the formation of an amorphous layer whose Raman phonon intensity is zero. As seen in Fig. 2c the crystalline factor is 0 for the non-annealed sample for probing wavelengths upto 531 nm. Then κ has some finite value and reaches a maximum of 0.14 at the deepest penetration depth. The behavior of the crystalline factor, as explained earlier, is simply due the probing depth of the Raman scattering signal. In the case of the short penetration depth due to the formation of the amorphous silicon layer the silicon phonon peak is not present ($\kappa = 0$). However, with increasing probing penetration depth the Raman signal is sampling a region outside the amorphous layer, thus giving some finite value for κ. The slightly annealed samples exhibit similar behavior. It is interesting to note in these samples (as seen in Fig. 3) the change of the crystalline factor from $\kappa = 0$ to $\kappa = 1$ occurs between 700 to 800°C.

Finally let us consider the highly doped silicon samples W5 and W6 namely the 5×10^{15} P^+/cm^2 and 1×10^{16} P^+/cm^2 phosphorus doped samples. These samples exhibit similar behavior as the 1×10^{15} P^+/cm^2 doped samples. The only difference now is that the samples crystallinity does not recover fully with annealing temperature even at temperatures higher than 800°C. This may be explained simply by the severe damage induced by the ion implantation at doses higher than the critical dose. The damage is also expected to be more pronounced closer to the surface of the samples since most of the damage will be induced when the ions have the highest energy. This effect is clearly seen in Fig. 2d, where the crystalline factor profile reveals a dip near the surface of the sample (note this effect is more pronounced for the higher doped sample W6). In fact, as it was shown in the past, in the case of implantation over the critical amorphization dose, even after high annealing of 800°C, one does not achieve complete recrystallization and annihilation of defects (for example, annealing between 800–1000°C is not sufficient to annihilate line and loops dislocations) [14].

Consider these data at each probing penetration depth as a function of doping level. It is clear from these results that with increasing doping level the crystalline factor κ decreases and approaches zero for higher doping levels. However, with increasing probing penetration depth, κ never reaches zero even for the higher doping levels. This is to be expected since the probing penetration depth becomes so deep that it exceeds the depth of the ion implantation.

4.2. Constant implantation dose

In this section we present and discuss the Raman scattering data for the silicon samples implanted at differ-

ent implantation energies at constant implantation dose of $5 \times 10^{14} P^{+}/cm^2$ which is less than the critical amorphization dose. Fig. 3 consists of 3 different graphs, corresponding to three different probing wavelengths. These graphs show the normalized phonon peak (or the crystalline factor κ, as we defined earlier) as a function of annealed temperature. One common feature in all these graphs (as well as the graphs for all the other wavelengths not shown here) is the transition point from $\kappa < 1$ to $\kappa = 1$ which seems to occur between 600 and 700°C (this was also observed in the past [15,16]). We also note that this transition is more pronounced for samples with implanted energies between

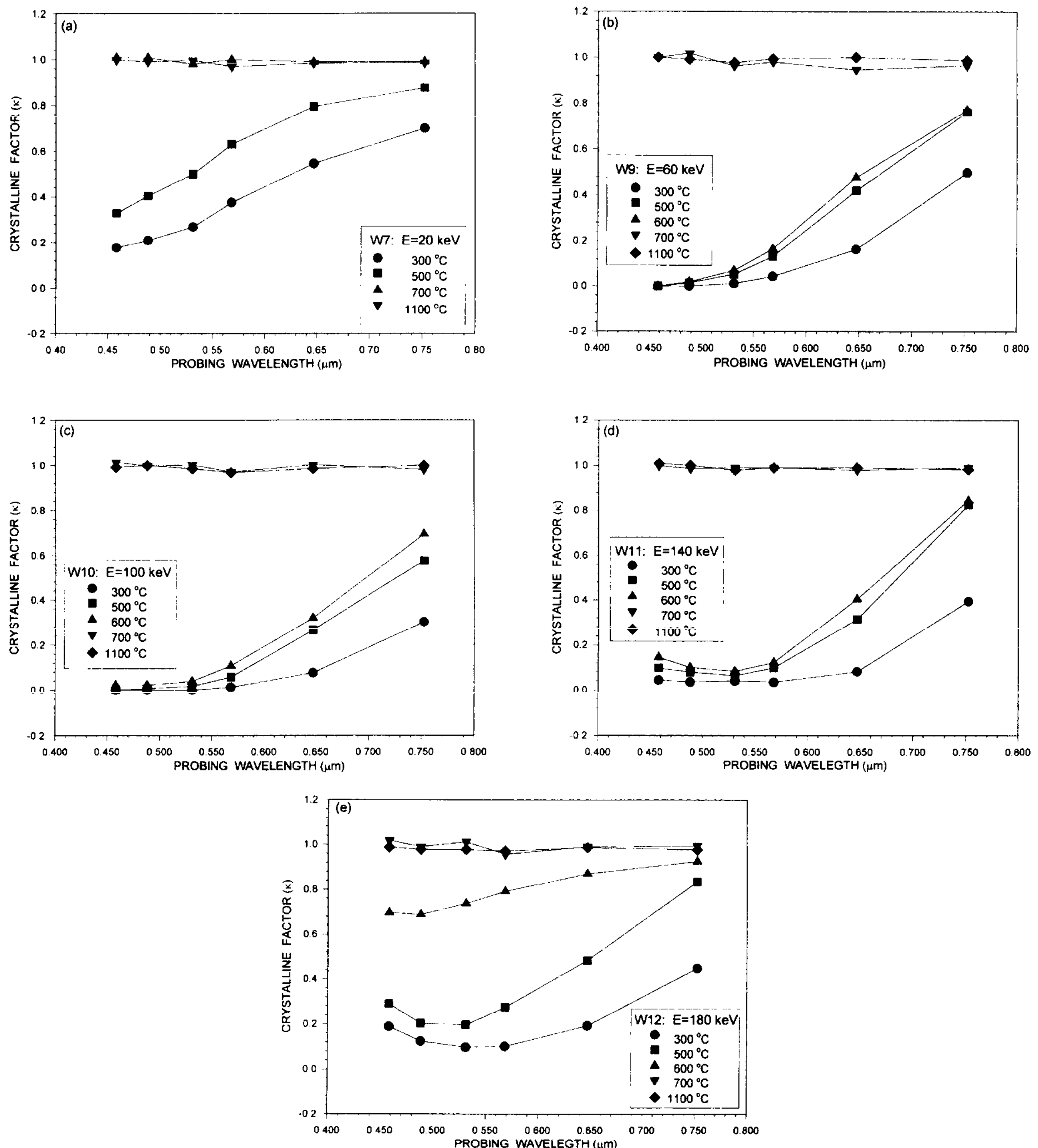

Fig. 4. The crystalline factor κ as a function of probing wavelength for different annealed temperatures. Parts (a) to (e) correspond to the different ion implantation energy samples, namely W7: 20 keV, W9: 60 keV, W10: 100 keV, W11: 140 keV and W12: 180 keV.

60 keV to 140 keV. Looking at these data as a function of wavelength this transition is less apparent as the penetration depth of the probing wavelength increases, as expected since the sampling depth region includes a deeper region unaffected by the implantation. It is also interesting to point out that the crystalline factor decreases as the implantation energy increases from 20 keV to 100 keV and then it starts to increase again. This may be explained as follows: during ion implantation a number of atoms (in the silicon lattice) is displaced and takes interstitial sites. The total number of atoms displaced by the projectiles of implantation energy E_0, is given by the following simple expression [14]:

$$N_t = \frac{P(E_0 - E_c) + bE_c}{E_d}, \qquad (2)$$

where $E_d = 15$ eV is the displacement energy for the target, $P = 10^{-3}$, $b = 1/2$ and in the case of silicon $E_c = 120$ keV. From the above equation we may calculate the number of interstitial silicon atoms versus ion implantation energy, E_0. We note that the number of interstitial silicon atoms is approximately the same for all the ion implantation energies of samples W7 to W12 (for example for low implantation dose $E_0 = 20$ keV, $N_t = 3993$ while for $E_0 = 180$ keV $N_t = 4004$). Since the displaced number of defects is almost the same for the range of implantation energies for the samples used in this experiment it seems that in the case of high implantation energies a part of this energy is dissipated locally in the lattice just as heat. It is possible that this local heating plays a role of local annealing which provokes a certain annihilation of some kinds of defects. For example, annihilation of a part of vacancy-P^+ defects which requires temperatures less than 100°C take place [14]. Thus, a number of these defects decreases with the increase of local temperature, therefore, the peak phonon for energies greater than 100 keV increases again.

Fig. 4 consists of five different graphs corresponding to samples W7, W9–W12. These graphs show the crystalline factor as a function of probing wavelength of the various samples.

Looking at the implanted samples with $E = 20$ keV as a function of wavelength it becomes apparent that the crystalline factor increases along with the penetration depth. For the unannealed sample $\kappa = 0.2$ at the shortest probing depth and reaches 0.7 at maximum probing penetration depth of approximately 3 μm. This increase in the crystalline factor as a function of probing penetration depth is seen in all the samples and it is simply due to the fact that with increasing probing depth the sampling region, which is not affected by the ion implantation, increases. Therefore, this will result in an increased crystalline factor.

It is also interesting to note in Fig. 4a the profile of the crystalline factor. It seems that most of the damage to the silicon lattice occurs close to the surface of the samples as one would expect. In fact, this was also confirmed with spreading resistance measurements as well as with theoretical simulations in these samples [11].

Similar results are also seen for the implanted samples at $E = 30$ keV except that the crystalline factor is now smaller than the previous sample, which is expected, since the implantation energy is larger, thus contribution to the creation of defects increases. The silicon samples implanted with phosphorus at $E = 60$ and 100 keV also exhibit the same behavior as the previous samples.

Samples W11 and W12 corresponding to implantation energies of 140 keV and 180 keV, respectively show some interesting features (see Fig. 4d and 4e). First the crystallinity factor is not zero even for the shortest penetration depth. Second, this value decreases to a minimum at 531 nm (deeper into the sample) and then it starts increasing again. We believe that this is simply due to local heating (or annealing) which contributes in the annihilation of some of the defects. This local annealing temperature is expected to be higher close to the surface where the ions are most energetic. Therefore, the contribution to annihilation of defects is larger close to the surface of the samples thus, resulting in a larger crystalline factor at the surface which drops with increasing penetration depth.

5. Conclusions

Raman scattering in the past has proved to be a very useful tool in probing ion implantation samples. In this work we demonstrate the importance of multi-wavelength Raman scattering which reveals information on the crystallinity of the ion-implanted samples as a function of probing depth. The introduction of the crystalline factor κ (Raman peak over the phonon Raman peak for the crystalline silicon) normalizes the Raman result and makes the analysis simple.

In summary, some of the interesting features revealed in this work for the different ion-implanted silicon samples are listed below. Damage caused by ion-implantation with small doses was minor and even low temperature annealing restored the samples back to their full crystalline structure. For these samples with doses less than the critical amorphization dose Raman scattering data revealed damage depths which extended over a few microns. Most of the damage in these samples was induced near the sample surface (a few hundred of nanometers away from the surface). Damage induced deeper into the sample recovered at lower temperature annealing than the damage caused at shallow depths.

The ion-implanted samples with dose higher than the critical amorphization dose formed an amorphous layer whose Raman phonon peak intensity was zero, thus, their crystalline factor was zero. At these implantation doses the crystalline factor never recovered fully even at temperature higher than 800°C due to the line and loops dislocations.

Raman scattering for the constant implantation dose samples (although lower than the critical amorphization dose) revealed damage to silicon lattice over 1 μm depth. Although with increasing, ion-implantation energies the damage depth increases, however the damage caused deeper into the sample was not as severe as the damage close to the surface of the samples. Most of the damage was recovered under high annealed temperatures even for the higher implantation energies. Also noteworthy was the transition from $\kappa < 1$ to $\kappa = 1$ which occurred between 600 to 700°C. In these samples evidence of local lattice heating for ion-implantation energies greater than 100 keV have been observed.

Finally, we like to point out that Raman scattering is indeed a powerful non-destructive technique for studying ion-implantation samples. However, using multi-wavelength probing makes this technique even more powerful and more useful due to the additional information obtained from probing the sample at various depths.

References

[1] H. Ryssel and I. Ruge, Ion-Implantation (Wiley, New York, 1986).
[2] C. Christofides, Semicond. Sci. Technol. 7 (1992) 1283.
[3] M. Balkanski, J.F. Morhange and G. Kanellis, J. Raman Spectrosc. 10 (1981) 240.
[4] B.L. Crowder, J.E. Smith, Jr., M.H. Brodsky and M.I. Nathan, Ion Implantation in Semiconductors (Springer, Berlin, 1971) p. 255.
[5] S. Ushioda, Solid State Commun. 15 (1974) 149.
[6] P.S. Peercy, Appl. Phys. Lett. 18 (1971) 574.
[7] H. Engstrom and J.B. Bates, J. Appl. Phys. 50 (1979) 2921.
[8] R.A. Forman, M.I. Bell and D.R. Myers, J. Appl. Phys. 52 (1982) 4337.
[9] K. Kirillov, R.A. Powell and D.T. Hodul, J. Appl. Phys. 58 (1985) 2174.
[10] T. Nakamura and T. Katoda, J. Appl. Phys. 53 (1982) 5870.
[11] A. Othonos, C. Christofides, J. B.-Said and M. Bisson, J. Appl. Phys. 75 (1994) 8032.
[12] W.C. Dash and R. Newman, Phys. Rev. 99 (1955) 1151.
[13] M.H. Brodsky, R.S. Title, K. Weiser and G.D. Pettit, Phys. Rev. B 1 (1970) 2632;
L. Crowder, R.S. Title, M.H. Brodsky and G.D. Pettit, Appl. Phys. Lett. 16 (1970) 205;
Lubbert and B.C. Burkey, J. Appl. Phys. 55 (1984) 760.
[14] J.F. Gibbons, Proc. IEEE 56 (1972) 1062.
[15] C. Christofides, A. Othonos, M. Bisson and J. B.-Said, J. Appl. Phys. 75 (1994) 3377.
[16] C. Christofides, H. Jaouen and B. Guibaudo, J. Appl. Phys. 65 (1989) 4832.